Global mass dependence of the isotope effect in diffusion

M. Marchese and C. P. Flynn
Department of Physics and Materials Research Laboratory, University of Illinois at Urbana-Champaign, 1110 West Green Street, Urbana, Illinois 61801
(Received 23 May 1988)

Using the short-memory augmented-rate theory (SM-ART) framework of Toller *et al.* [Phys. Rev. B **32**, 2082 (1985)] we have calculated the isotope effects for diffusion in crystals over wide ranges of the mass of the jumping atom relative to that of the host atom. Calculations have been completed for a variety of interatomic potentials including Lennard-Jones, Morse, Finnis-Sinclair, and hard-core forces. The similar global behavior in all cases points to the dominance of closed-shell repulsive forces in determining the isotope effect for diffusion. These results also clarify the expected behavior of the isotope effect for impurity diffusion in which large mass differences are present. An example of the breakdown of the SM-ART approximation is discussed.

I. INTRODUCTION

In recent work with collaborators we have been able to explain the isotope effects for diffusion observed at high temperature in fcc (Ref. 1) and bcc (Ref. 2) metals. The general framework for this research is provided by a theory due to Toller *et al.*[3] designated the short-memory augmented-rate theory (SM-ART). Earlier applications of classical statistical mechanics to this problem resulted in the Vineyard theory,[4] in which the rate at which transitions take place is predicted from the single-time statistical distribution function. In this simpler framework the isotope effect is fixed[5] by the orientation of the "saddle surface" on the top of the barrier barring the jump path in configurational space. Unfortunately, model calculations that determine the saddle plane normal in terms of interatomic forces yield results that are in substantial disagreement with the observed isotope effects.[1] The SM-ART treatment includes, in addition, the dynamics[3] of trajectories close to the jump condition, and thereby corrects errors of jump counting that occur in the simpler treatment. It turns out that the mass dependence of these errors is the dominant factor in the isotope effect. The present paper uses the SM-ART framework to examine the global behavior of the isotope effect over large changes of isotope mass, lattice characteristics and temperature.

An important feature of the SM-ART treatment is that it eliminates spurious counting of atomic jumps. In rate theory the number of trajectories per unit time that cut the saddle surface is counted without reference to their future behavior. The SM-ART theory, in contrast, treats trajectories close to the jump condition in a way that is, in principle, exact, so that immediate reversals are eliminated. The locus of all trajectories that oscillate indefinitely on the top of the barrier in phase space is called the center manifold (CM) of the barrier. Trajectories that differ from this by an infinitesimal velocity, so that they decompose from CM, form the center unstable manifold (CS^-), and their time reversed trajectories form the center stable manifold (CS^+). The flow of trajectories around these manifolds in phase space is illustrated schematically in Fig. 1. Any surface Σ^+ that extends from CS^+ to region of inaccessibly high-energy cuts all the flux in one sense; trajectories that reverse are trapped between CS^+ and CS^- so they do not contribute at that time to the flux through Σ^+. This eliminates the principal error that is inherent in the rate-theory approach.

Figure 1 makes clear that the SM-ART treatment focuses on short dynamical processes involving trajectories close to CS (not necessarily short times[6]). It does not, for example, eliminate trajectories that pass around CS^+ and CS^- before contributing a return jump through Σ^-. Nor does the theory include possible turbulence of the flow lines of the trajectories. These fundamental topics are not the subject matter of this paper, and are neglected here except for some brief discussion of the chaotic behavior we have found for certain models of bcc metal. These latter results are collected in the Appendix.

Calculations of the isotope effect have been reported elsewhere for simple fcc and bcc metals.[1,2] The methods by which the SM-ART treatment is realized in practice are reviewed briefly in Sec. II. For fcc metals the error in rate theory, as specified by a conversion coefficient c that is unity when no error occurs, is negligible at low temperature and, in fact, c deviates from unity at high temperature only by $\sim 10\%$ for fcc and 30% for bcc lattices. Thus, rate theory is a satisfactory first approximation. Nevertheless, corrections are required to bring the calculated isotope effect into agreement with experiment. The isotope effect κ is unity for independent motion of the jumping atom and is smaller when other atoms participate in the jump dynamics. For fcc Cu, Ag, and Ar, represented by fitted Morse and Lennard-Jones potentials, the calculated SM-ART isotope effect factor decreases from a rate theory value of about 0.96 at $T=0$ to about 0.88 near T_m. The value near T_m, where most measurements are made, agrees well with the experimental results for these metals and, more generally, for the observed behavior of a wide range of close packed sys-

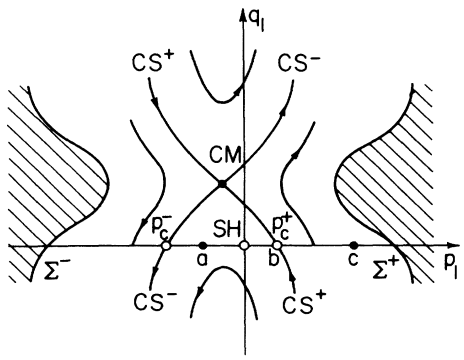

FIG. 1. Sketch showing the center stable (CS^+) and center unstable (CS^-) manifolds intersecting at the center manifold CM. The saddle hyperplane SH, comprising the saddle plane and all velocities that lie in it, has dimensionality $6N-2$ as in CM. Added critical perpendicular momenta, p_1^+ and p_1^-, give trajectories on CS^+ and CS^-. For $p_1 > p_1^+$, e.g., point c, a transition takes place, but for $p_1 < p_1^+$, e.g., point a, the trajectory is simply a fluctuation from the initial potential well. All successful transitions cut an arbitrary surface Σ^+, that extends from CM to regions of large energy, an odd number of times.

tems.[7] For bcc Fe the observed $\kappa=0.59$ at high temperature[8] is reproduced well by the theory with a Finnis-Sinclair potential,[9,2] fitted to α-Fe, which gives a small double peaking of the potential energy along the jump path. The conversion coefficient is again reasonably close to unity at about 0.71. For both the fcc and bcc structures, the theory shows that the isotope effect is dominated by a temperature-dependent fraction of highly anharmonic trajectories.

The present work was undertaken to resolve certain broad questions raised by these results. One puzzle, for example, is how the isotope effect factor can be modified so strongly while the conversion coefficient itself remains close to unity. A second question concerns the behavior for large mass changes, which in practice require studies of impurity diffusion. To characterize these processes it is necessary to examine the global behavior of the conversion coefficient as the mass of the jumping atom, relative to that of the host atom, is varied over a wide mass range. In what follows we report an investigation of these properties. The theoretical methods and their application are described in Sec. II. Section III is a discussion of the results. A brief summary of the paper is given in Sec. IV.

II. ISOTOPE EFFECT CALCULATIONS

In other work,[3,6] we have established certain results that are exact within the SM-ART approximation. One is that the jump rate may be written

$$R = R_0 c \ , \tag{1}$$

with R_0 the jump frequency calculated by rate theory for a planar saddle surface normal to the decomposition mode at the saddle point, and c a "conversion coefficient" that measures the fraction of saddle plane crossings that lead to actual jumps (i.e., $1-\eta$, with η the fraction of unrandomized return jumps). The isotope effect factor follows as

$$\kappa = -2\frac{\partial \ln R}{\partial \ln M_1} \ , \tag{2}$$

or

$$\kappa = \kappa_0 - 2\frac{\partial \ln c}{\partial \ln M_1} \ , \tag{3}$$

where κ_0 is the rate theory (harmonic) isotope effect factor and M_1 is the mass of the moving atom. In Eqs. (2) and (3), all masses other than M_1 are held constant.

A second exact result is that κ_0 is given by the directional cosines of the saddle plane normal in configurational space relative to the subspace of the jumping atom.[5,6] Thus

$$\kappa_0 = \frac{\sum_{\alpha=1}^{3} a_{1,\alpha} M_1^{-1}}{\sum_{i=1}^{N}\sum_{\alpha=1}^{3} a_{i,\alpha} M_i^{-1}} \ , \tag{4}$$

with the $a_{i,\alpha}$ directional cosines of the saddle surface normal. In Eq. (4) the index is summed over all the atoms and the index α identifies their Cartesian coordinates.

Our earlier calculations of κ for fcc and bcc crystals evaluate $\kappa(M_1)$ for a mass M_1 of the jumping atom equal to that, M, of the host atom. For this purpose an accurate difference algorithm was devised to determine small changes of conversion coefficient caused by small changes of M_1 with respect to M. For our present purpose the earlier difference algorithm no longer serves well. By methods outlined below we have therefore made direct calculations of c and of κ as functions of M_1/M, so that the full isotope effect and its mass dependence can be derived from Eq. (3).

The procedures by which κ_0 may be obtained are straightforward. The dynamical matrix is diagonalized at the saddle point and the orientation of the unstable mode then determines directly the relevant cosines, and hence κ_0. Its value is mass dependent both through the explicit masses in Eq. (4) and through the presence of the masses in the dynamical matrix. The latter corresponds to the fact that the normal-mode directions in configurational space depend on all the masses present. Values of κ_0 for various interatomic potentials presented below are based on this prescription.

Our procedure to find the second, "anharmonic," contribution to the jump rate begins with the selection of an ensemble of representative points on the saddle hypersurface in phase space. This may be accomplished with equal convenience either by molecular-dynamics (MD) or Monte Carlo (MC) methods. The saddle hyperplane (SH) comprises the saddle plane together with all momenta that lie in that plane. As such it has the dimensionality of CM ($6N-2$, with N the number of atoms) but is generally distinct from it. Thus SH and CM appear as separate points in the schematic Fig. 1. Any state on SH

can be brought onto CS^+ by an increment p_c of momentum perpendicular to the saddle plane. By construction, any state on SH with added perpendicular momentum $p > p_c$ then gives rise to a jump (e.g., point c in Fig. 1). Thus, we first identify p_c as the momentum that makes a state initially on SH approach the barrier and linger there indefinitely. The integral over Σ^+ is obtained by repeating this procedure for the ensemble of states on SH. In practice, we determine the *fraction* of all available p values that lie between $p = p_c$ and ∞, and thus obtain the conversion coefficient directly. In this way we have obtained c as a function of M_1/M for several different interatomic potentials.

In all cases of a simple single barrier we have found that, to the accuracy of our calculations, there exists a unique critical momentum p_c below which all trajectories fail and above which all trajectories for a given state on SH lead to successful jumps. The precision with which this observation holds is $\sim 10^{-5}$ of the mean thermal momentum perpendicular to SH, which is the limiting accuracy of our trajectory calculations. In the case of the double barrier for the bcc vacancy jump, referred to below, we found a completely different behavior. For this case alone, and only at sufficiently low temperature, successful and unsuccessful trajectories were found to be interleaved with increasing p, so that the selection of a unique p_c proved impossible. These phenomena relate in an interesting way to a chaotic behavior of the flow lines associated with the randomization of trajectories within the well of the double barrier. A brief description of these results is presented in the Appendix.

We now present the results of calculations performed for particular systems using the methods outlined above. Vacancy hopping has been investigated for both fcc and bcc lattices using potentials that are appropriate to the two cases. Specifically, for the bcc lattice we have employed the model Finnis-Sinclair potential fitted in our earlier work[2] to the parameters that describe phonon and defect properties of α-Fe. For the fcc lattice we employ a Lennard-Jones model from our earlier studies, which is fitted to the properties of Ar. Details of the precise parameters that describe the potentials may be found in the original papers.[10,3] For the main part calculations were confined to a 32-atom fcc cluster and a 54-atom bcc crystallite, both with periodic-boundary conditions and the largest cutoff available for the specific system. Even so, the calculations were extensive, requiring runs of many (10–30) hours on an FPS 264 attached processor.

Figure 2 summarizes the calculated conversion coefficients as a function of the logarithm of mass ratio for a wide range of M_1/M. While all the data in Fig. 2 correspond to a temperature close to the melting point of the material being simulated, we have verified in auxiliary calculations that c exhibits a qualitatively similar mass dependence at other temperatures also. The most important observation is that the conversion coefficient changes rapidly with M_1 for $M_1/M \sim 1$ and eventually becomes independent for M_1 for M_1/M sufficiently large or small (viz, $> 10^2$ or $< 10^{-2}$). The actual computed values, together with their uncertainties, are collected in Table I.

Our earlier investigations have revealed that the isotope effect behavior is dominated by hard-core effects. For this reason we have extended the present calculations to a model which exhibits these characteristics clearly. In this model the harmonic potential of the potential barrier close to the saddle point is extended to all of configurational space. It is supplemented by an infinite repulsion of range σ between the jumping atom and all others. Thus the true anharmonic potential is simplified as a harmonic potential plus rigid-core effects. For the Lennard-Jones fcc crystal near $M_1/M = 1$ this has been found earlier[1] to mimic both the conversion coefficient c and isotope effect κ of the conventional potential very satisfactorily, for values of the core radius σ that are appropriate for the observed bulk anharmonicity.[11] Since the harmonic force without the rigid core gives both c and κ quite incorrectly, it may be deduced from the subsequent agreement that the major discrepancies arise from hard-core effects. In the present research these re-

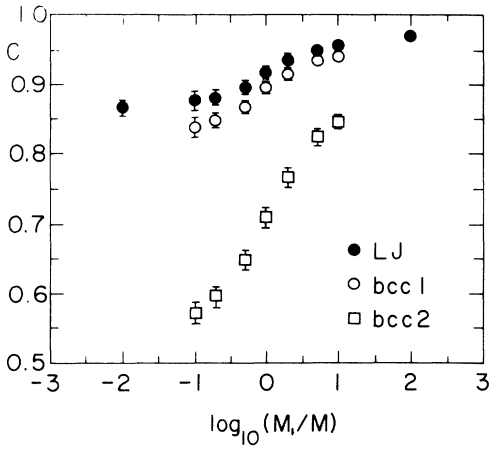

FIG. 2. The conversion coefficient as a function of M_1/M shown for three different potentials. LJ, fcc Lennard-Jones; bcc 1, single-peaked Finnis-Sinclair; bcc 2, double-peaked Finnis-Sinclair. In this and following figures the mass scale indicates a power of 10.

TABLE I. Conversion coefficients as functions of mass ratio M_1/M for the fcc Lennard-Jones model, for the single and double bcc Finnis-Sinclair potentials, and the hard-core potential, discussed in the text.

Mass	Lennard-Jones	Hard core	Single bcc (1 peak)	Double bcc2 (2 peaks)
0.01	0.865	0.863		
0.10	0.876	0.870	0.838	0.572
0.20	0.881	0.879	0.847	0.595
0.50	0.897	0.899	0.867	0.648
1.00	0.918	0.921	0.896	0.710
2.00	0.938	0.940	0.917	0.766
5.00	0.950	0.955	0.937	0.823
10.00	0.958	0.964	0.943	0.846
100.00	0.969	0.971		

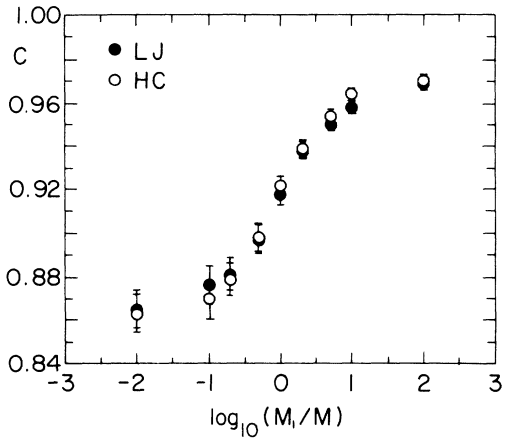

FIG. 3. Comparison of conversion coefficients for fcc crystals with different interatomic force laws. LJ, Lennard-Jones; HC, harmonic with hard core.

sults have been extended to obtain the overall dependence of c on M_1/M for this same rigid-core potential applied to the Lennard-Jones model fcc crystal. These results are displayed in Fig. 3 where it can be seen that the calculated variations of c are entirely analogous to those of the realistic Lennard-Jones potential. We note again that this behavior must arise from the rigid core since the harmonic term alone gives a constant value of c near unity for all M_1/M.

We turn finally to the variation with M_1/M of the harmonic and anharmonic contribution to the isotope effect. As an example the value of κ_0 calculated for the fcc lattice with the Lennard-Jones potential is shown as a function of $\ln(M_1/M)$ in Fig. 4(a). From a numerical differentiation of the conversion coefficient mass dependence it is then possible to obtain the anharmonic contribution corresponding to the second term in Eq. (3). This term added to κ_0 gives the full isotope effect factor which is shown as the solid line in Fig. 4(a). Notice that the anharmonic term makes its main contribution near $M_1=M$, whereas the term κ_0 shows a monotonic variation all the way from $M_1 \ll M$ to $M_1 \gg M$. Figure 4(b) gives the analogous results for the potential used above to represent bcc α-Fe. The qualitative features of the results are similar to those for the fcc case, although the quantitative deviations of κ from unity are of course larger in the bcc case.

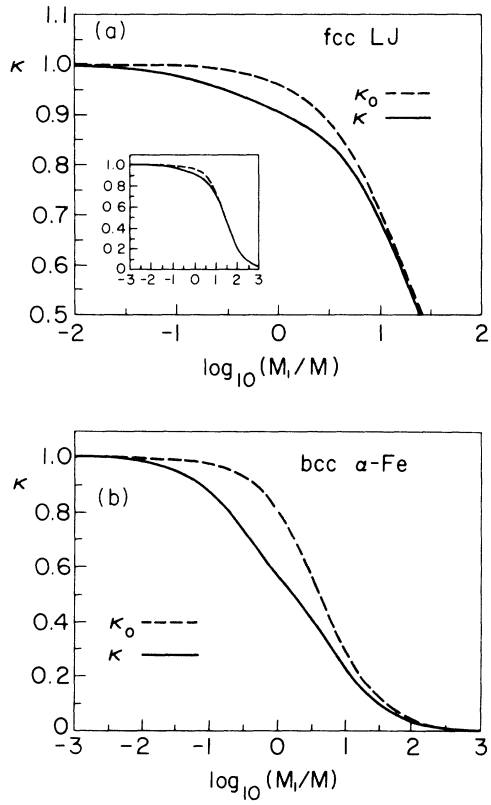

FIG. 4. Isotope effect as a function of M_1/M for (a) Lennard-Jones fcc crystal and (b) Finnis-Sinclair best fit for bcc α-Fe. In both figures the harmonic contribution separately is indicated by the dashed line, and the total by the solid line.

III. DISCUSSION

In this discussion of the results presented above our main purpose is to provide insight into two features of these calculations. These are, respectively, the physical origins of the anharmonic term and the expected behavior of impurity systems in which the mass of the diffusing atom differs widely from that of the remaining atoms. These two areas are discussed successively in what follows.

With regard to the anharmonic term we note first that the results presented in Sec. II explain very directly how its contribution to the isotope effect can be large while the conversion coefficient remains close to unity. In the diverse cases shown in Figs. 2 and 3, all the conversion coefficients change most rapidly with mass precisely in the region $M_1 \sim M$, where measurements of the isotope effect in *self*-diffusion is necessarily determined. For this reason the anharmonic contribution to the isotope effect near $M_1=M$ has the same typical size as the deviation of the conversion coefficient from unity, which is much larger than the deviation of κ_0 from unity near $M_1=M$. The net result is that the full isotope effect near $M_1=M$ has a dominant contribution from the anharmonic term. This is not the case when M_1 is very different from M, as discussed in more detail below, after further analysis of the anharmonic contribution.

The global character of the anharmonic term in κ is established unambiguously by Fig. 5. This figure shows that the two bcc and two fcc systems represented in Figs. 2 and 3 all give rise to the same functional form of the anharmonic term. In Fig. 5 the variations with M_1/M have been scaled to the same amplitude and shifted in height, so that the changes from M_1/M small to M_1/M large are similar for all four systems. It is apparent that the results for the different systems have identical dependencies on M_1/M, within the small uncertainties of the computational results. The precise scale shown in Fig. 5 is chosen so that a line representing the reduced mass

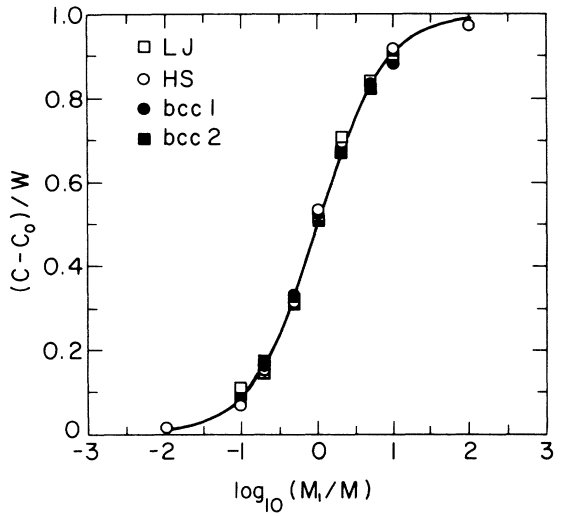

FIG. 5. The conversion coefficients from Figs. 2 and 3 shifted and scaled by factors w to make them fall close to a common trend. The line shows the variation of $\mu = MM_1/(M+M_1)$.

$$\mu = \frac{MM_1}{M+M_1} \tag{5}$$

passes through the data. Now the reduced mass is pertinent to energy transfer in two-particle collisions between the jumping atom of mass M_1 and its neighboring host atoms of mass M. It is useful to recall, in addition, that for one set of data in Fig. 5 the mass dependence is almost entirely the consequence of rigid repulsive forces between the diffusing atom and the remaining lattice atoms. Thus, Fig. 5 provides conclusive evidence that the anharmonic isotope effects described here arise in major part from the influence of core forces on the probability with which unrandomized return jumps take place. Numerical values of c for different mass ratios are collected in Table I.

The final picture of the isotope effect that emerges from these studies is thus very different from the views that prevailed until very recently, but nevertheless one that can be expressed in simple physical terms. It has been demonstrated that anharmonic effects due to deep closed shell collisions exert a dominant influence. The value of κ_0 is close to unity throughout a wide range of M_1 that spans M. This shows that the decomposition mode at the saddle point, along which low-energy trajectories pass, lies almost wholly in the subspace of the migrating atom. For $M_1 \ll M$, deep collisions between M_1 and its neighbors scatter the system far out of this subspace into other jump directions that involve less motion of M_1. These events reduce the sizes of the conversion coefficient for M_1 small. As M_1 is increased to exceed M, however, this scattering becomes less effective, the conversion coefficient increases, and the decomposition motion scatters less out of the M_1 subspace. Because the conversion coefficient thus increases with M_1 the anharmonic term give a negative contribution to κ. The effect is large only near $M_1 = M$ because this is the domain in which the effectiveness of the hard-core scattering changes from one regime to the other.

We turn now to the expected behavior of the isotope effect for diffusion of atoms with masses very different from the host atom mass. In practice, this must necessarily be impurity diffusion. The model forces employed above are not generally suitable for this case because the impurity-host interaction may in general be expected to differ from the host-host forces, which is not the case for the models described in Sec. II. We believe that some of the physical characteristics revealed by the calculations will nevertheless remain relevant to the case of impurity diffusion. In particular, the fact that the anharmonic effect from deep collisions becomes of negligible importance when M_1 differs greatly from M should carry over to impurities also. This is the case because the behavior is a consequence of the mass ratio and the hard-core forces alone, so that the general strength of the bonding is not relevant. The isotope effect observed for impurities with masses very different from the host mass must therefore be determined mainly by the harmonic term κ_0. Thus the impurity case for large mass differences is the exact opposite of the situation for host atoms described above.

As κ_0 is expected to vary in a specific manner with M_1/M, we are now able to make qualitative predictions about the isotope effect for impurity diffusion. When the jumping impurity is very light, for example, the decomposition mode must lie almost wholly in the subspace of M_1. It follows for $M_1/M \to 0$ that $\kappa \to 1$. For sufficiently large M_1, on the other hand, the fast motion of neighbors must play an increasingly large role in promoting jumps, and for $M_1/M \to \infty$, κ_0 must tend to zero. Finally, for impurities of intermediate mass, M_1, close to the mass M of the host atoms, the behavior must again be modified by the anharmonic contribution, and the isotope effect factor κ takes a value similar to that for self-diffusion. These are indeed the qualitative features revealed by Fig. 4. It is our belief that the global behavior does not depend in a critical way on the fact that impurity-host forces must differ from host-host forces. Therefore the trend in Fig. 4 provides a qualitative guide to the isotope effect for impurity diffusion also.

Experimental results for the isotope effect of impurities with M_1/M very large or very small are not yet available for comparison with these predictions. Future efforts might, with advantage, focus on cases such as heavy impurities in Li, and Li in heavy-host lattices, where mass ratios of order 30 appear to be accessible for study. These should be sufficiently large that the mass ratio overshadows effects of local impurity-host interactions, and that the global behavior described above [Figs. 4(a) and 4(b)] dominates the isotope effect.

IV. SUMMARY

By means of model calculations based on the SM-ART approximation we have examined the dependence of the isotope effect factor κ on the mass M_1 of the migrating atom, relative to the mass M of host atoms, over a wide

range of M_1/M. In the region $M_1 \sim M$ relevant to self-diffusion the isotope effect is dominated by an anharmonic contribution caused by hard core collisions that take place between the migrating atom and its neighbors during the jump process. These scattering events reduce the conversion factor for M_1 small, and therefore give a negative contribution to κ in the region $M_1 \sim M$. On the other hand, for impurity diffusion with M_1 very different from M, the anharmonic contribution is expected to be small. Then $\kappa \sim \kappa_0$, and the isotope effect must vary from near unity for $M_1/M \to 0$ to near zero for $M_1/M \to \infty$, as does κ_0.

ACKNOWLEDGMENTS

Thanks are due to G. Jacucci, G. DeLorenzi, and M. Toller for their contributions to the models used in this research. Support from the National Science Foundation (NSF) through University of Illinois Materials Research Laboratory Grant No. DMR-86-12860 is acknowledged.

APPENDIX

The SM-ART treatment is based on the presumed smooth behavior of the flow lines close to the center manifold. Even for simple systems it cannot be expected that the trajectories necessarily behave monotonically as a function of some momentum coordinate, once they pass around either CS^+ or CS^- to lie in the region of oscillating motion. Rather, smooth behavior is guaranteed only in the neighborhood of CM on jump trajectories that pass through the harmonic potential close to the saddle point.

We have explored this point to a limited extent by studying trajectories close to $p = p_c$ for some members of an ensemble initially selected on SH, in accordance with the discussion of Sec. II. Figure 6(a) shows the typical behavior. Trajectories with p close to p_c adhere accurately to the same path for a long-time interval before veering over to one equilibrium site or the other. The two trajectories shown differ by only ~ 0.0003 of the mean thermal momentum. The sharpness of the transition from one future location to the other is further illustrated in Fig. 6(b). There, the time at which the future location becomes clearly apparent is shown for a continuum of trajectories near p_c. An unambiguous transition from one fate to the alternative one is found to occur abruptly within the computational resolution of $\delta p_c \sim 10^{-5}\langle p \rangle$, with $\langle p \rangle$ the mean thermal momentum at the temperature chosen for the calculation.

Our calculations for bcc metals in the case of a double-peaked potential barrier reproduce the experimental high-temperature isotope effect[2] satisfactorily. Within the precision of calculation we again observe that, at high temperatures, a unique p_c can be identified for transitions over the double peak. At lower temperature, however, when the thermal energy per particle becomes comparable with the well depth between the peaks, we observe that the fate of individual trajectories no longer depends so simply on p in the neighborhood of p_c. Indeed, a unique value of p_c can no longer be identified. Figure 7(a) shows a typical series of trajectories with systematically varying p where the fate of an apparently critical trajectory is changed progressively from one final state to the other. The chaotic nature of the transition is more clearly evident in Fig. 7(b). This shows the times at which the fates of trajectories near p_c become apparent, in a way analogous to Fig. 6(b). Unlike the former example, however, no sharp transition occurs. Instead, trajectories with opposite fates are interleaved over a substantial range of p. Thus a transition to a chaotic regime of behavior appears to have taken place.

It is clear that the observed effects are connected with the randomization of trajectories that oscillate in the potential dip on top of the barrier. At sufficiently low temperatures complete randomization is expected. Exactly half the transitions over one peak to the dip will retrace the initial step. Since this applies to all isotopes, the isotope effect in the jump rate for $T \to 0$ must be just the isotope effect for either of the peaks separately. This value is κ_0 for the particular peak, as the anharmonic term must become negligibly small at low temperatures.

At present we lack methods to calculate the isotope effect in the intermediate regime above $T = 0$ where κT is

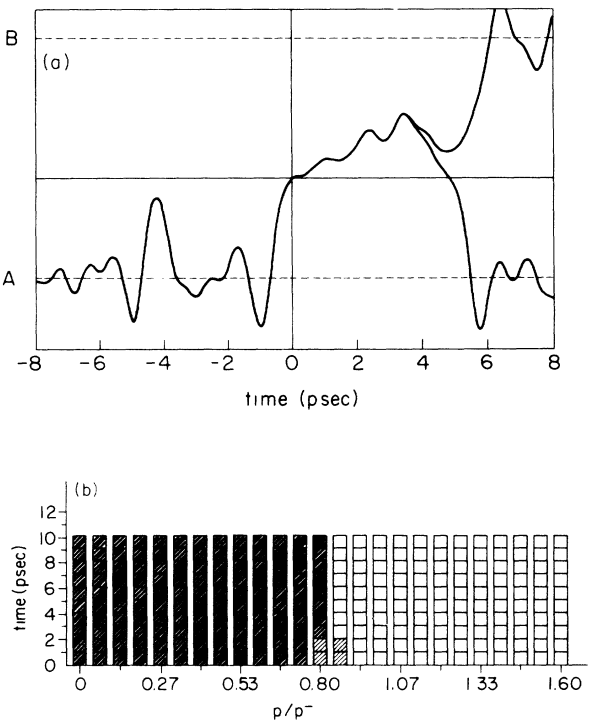

FIG. 6. (a) At high temperature for the double-peaked potential, trajectories with slightly differing perpendicular momenta of 0.13677 and 0.13673 depart to opposite fates after a long common trajectory. The mean thermal value of p for this example is $p = 0.15$. (b) The times at whch the fate becomes evident for a series of trajectories with differing perpendicular momenta. The approximate positions of the well bottoms in (a) are marked A and B. Dark and light boxes in (b) pertain to these wells as eventual equilibrium sites.

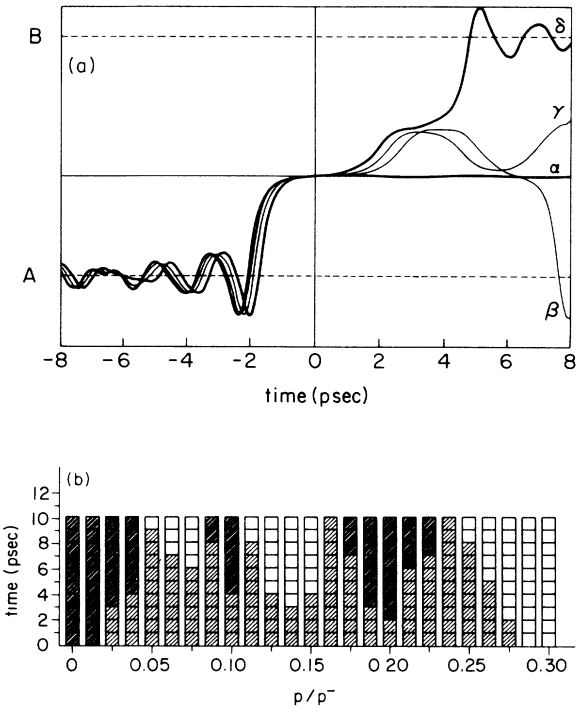

FIG. 7. (a) At low temperature ($\frac{1}{5}$ of the dip) for the double-peaked potential, the fates of trajectories vary unsystematically with perpendicular momentum through the series $\alpha,\beta,\gamma,\delta$ (α apparently lies on CS^+). (b) The times at which the fates become apparent also vary erratically with $p_\perp$ and no unique p_c is evident. For this example the mean thermal momentum is $p=0.08$. The approximate positions of the well bottoms are marked A and B.

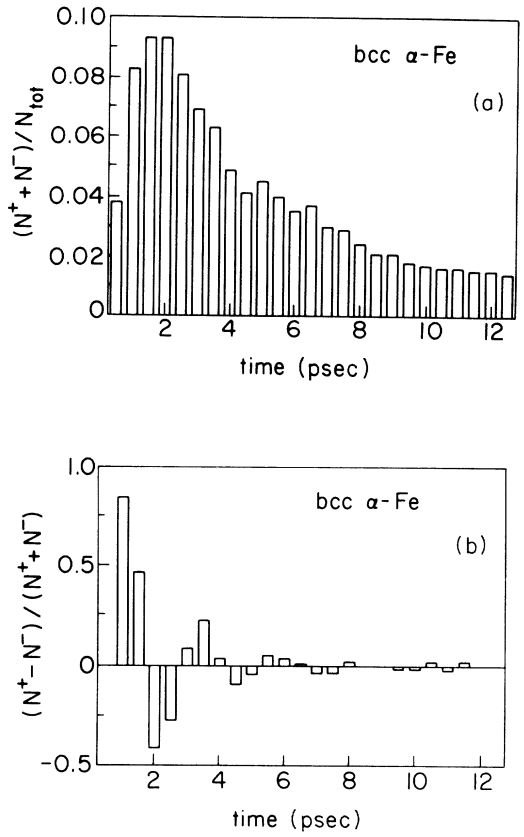

FIG. 8. Times at which transitions take place over the two peaks of the double barrier (a) summed, as a fraction of the total jumps, and (b) the fractional difference, showing how dephasing damps the oscillation faster than the escape rate in (a).

comparable with the potential dip. The results of some further investigation of this regime are displayed in Fig. 8. In order to examine the randomization process itself we define quantities $N_+(t)$ and $N_-(t)$. Given an ensemble of systems that initially cross a particular peak at time $t=0$, $N_+(t)dt$ and $N_-(t)dt$ measure, respectively, the numbers that pass over the second peak and the number that pass back over the initial peak in the time interval $t\rightarrow t+dt$. Figure 8(a) shows how $N(t)=[N_+(t)+N_-(t)]/N$ varies with time at $T=\frac{1}{5}T_0$, with $T_0=0.02$ eV the depth of the dip. The time ~ 6 ps taken for $N(t)$ to fall off to e^{-1} of its initial amplitude measures the decay rate of states out of the potential dip by transitions over one or the other of the peaks. Also shown in Fig. 8(b) is the quantity

$$P(t)=\frac{N_+(t)-N_-(t)}{N(t)} \tag{A1}$$

The different states are started out in phase as they cross the initial peak. Therefore $P(t)$ gives some measure of the way the ensemble dephases to spread across the phase space available to state in the dip. It is apparent that the dephasing is much faster that the escape rate, so that the system has time to randomize and produce chaotic interleaving of future transitions over the alternative peaks. From our results at high temperature, we conjecture that for $T\gg T_0$ the escape rate must exceed the dephasing rate. Under those circumstances, the chaotic behavior can no longer dominate the dynamics and the system must act then as if it has a single center manifold.

[1]M. Marchese, G. DeLorenzi, G. Jacucci, and C. P. Flynn, Phys. Rev. Lett. **57**, 3280 (1986); M. Marchese, G. Jacucci and C. P. Flynn, Phys. Rev. B **36**, 9469 (1987).
[2]M. Marchese, G. Jacucci, and C. P. Flynn, Philos. Mag. Lett. **57**, 25 (1988).
[3]M. Toller, G. Jacucci, G. DeLorenzi, and C. P. Flynn, Phys. Rev. B **32**, 2082 (1985).
[4]G. H. Vineyard, J. Phys. Chem. Solids **3**, 121 (1957).
[5]C. P. Flynn, Phys. Rev. Lett. **35**, 1721 (1975); C. P. Flynn and G. Jacucci, Phys. Rev. B **25**, 6225 (1982).
[6]G. Jacucci, G. DeLorenzi, M. Marchese, C. P. Flynn, and M. Toller, Phys. Rev. B **36**, 3086 (1987).

[7]N. L. Peterson, in *Diffusion in Solids,* edited by A. S. Nowick and J. J. Burton (Academic, New York, 1975), and references therein.
[8]C. M. Walter and N. L. Peterson, Phys. Rev. **17**, 922 (1969).
[9]M. W. Finnis and J. E. Sinclair, Philos. Mag. **A50**, 45 (1984).
[10]G. DeLorenzi, G. Jacucci, and C. P. Flynn, Phys. Rev. B **30**, 5430 (1982).
[11]L. Verlet, Phys. Rev. **165**, 209 (1968).